Copyright © 1982 American Telephone and Telegraph Company
THE BELL SYSTEM TECHNICAL JOURNAL
Vol. 61, No. 9, November 1982
Printed in U.S.A.

A Theoretical Model of Transient Heat Transfer in a Firestopped Cable Bundle

By P. B. GRIMADO

(Manuscript received April 7, 1982)

A mathematical model of heat transfer in a firestopped vertically oriented cable bundle is derived to assist in planning fire test experiments and to enumerate how changes in geometric and thermophysical properties affect the temperature rise in the cables when subjected to standard furnace fire tests. The analysis indicates that the primary heat transfer mode to the cable array is from the flow of hot furnace gases up through the void spaces between the individual cables. As expected, the most practical and effective way of reducing the heat transmission characteristics of a cable bundle is by tightly packing the firestop, which reduces the void space between cables and provides heat sinking to the cooler environs.

I. INTRODUCTION

In this paper a mathematical model of heat transfer in the cable bundle of a firestopped vertical cable assembly is developed to assist in planning experiments and to evaluate the relative influence of the geometrical and thermophysical properties of this portion of the firestopped configuration. A representation of this complex cable bundle geometry in terms of an approximate transient one-dimensional, lumped parameter model is obtained through heuristic arguments. This is accomplished in a systematic way by first deriving a simplified model for a single conductor wire and progressing up in scale, by averaging and lumping parameters, to arrive at a heat transfer model of a single cable. The heat transfer in a cable bundle is then treated using the single-cable model. Cable-to-cable heat transfer is handled through boundary conditions at the contact surfaces of the individual cables. A set of coupled transient one-dimensional equations results, with as many equations as cables in the array. The model is then exercised to compute transient temperature distributions within a

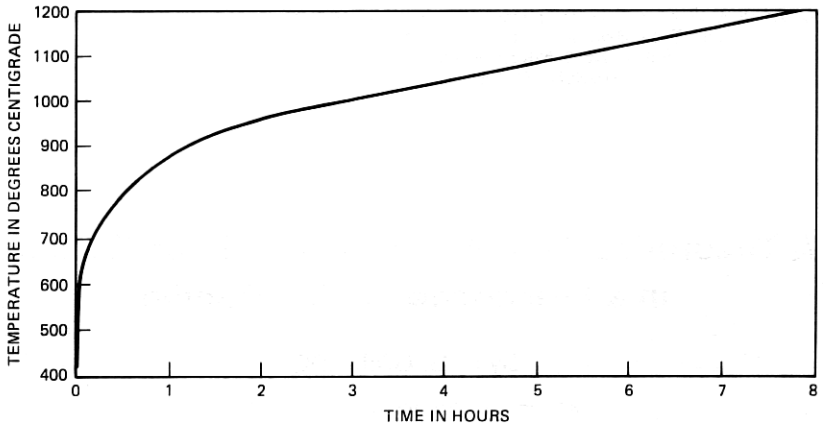

Fig. 1—ASTM E119 standard temperature vs time curve.

vertically oriented firestopped cable bundle when exposed to the ASTM E119* temperature variation shown in Fig. 1.

Properties of three generic-type cables (terminating, switchboard, and power cable) are used to suggest how physical and geometrical characteristics of the cables influence the effectiveness of a firestopped cable closure. It should be noted that an absolute evaluation of a firestop using the approximate heat transfer model developed here is beyond the capability of the model. This can only be attempted when considering potential nonlinear combustion modes of the polymeric cable materials, which is beyond the scope of this paper.

II. HEAT CONDUCTION MODEL OF A SINGLE CABLE

A cable consists of a core containing the insulated wire conductors and an outer protective sheath. In general, the cable core will contain a loose array of copper wires (which constitute 40 to 50 percent of the core) covered with a thin, polymeric insulating layer. The dominant path of heat conduction, because of their high conductivity, is in the longitudinal direction of the copper wires. Heat is also transferred radially, through the porous array of wires, by virtue of thermal radiation and heat conduction through contact points along the length of the wires, as shown in Fig. 2. The cable core cannot be considered a continuum because of the noncontiguous nature of the wires; hence, in developing the governing equation of heat conduction it is desirable to consider the individual wires as microstructural elements. This concept, as will be seen, permits interaction of the wires and leads, in

* Standard Methods of Fire Tests of Building Construction and Materials, American Society of Testing Materials.

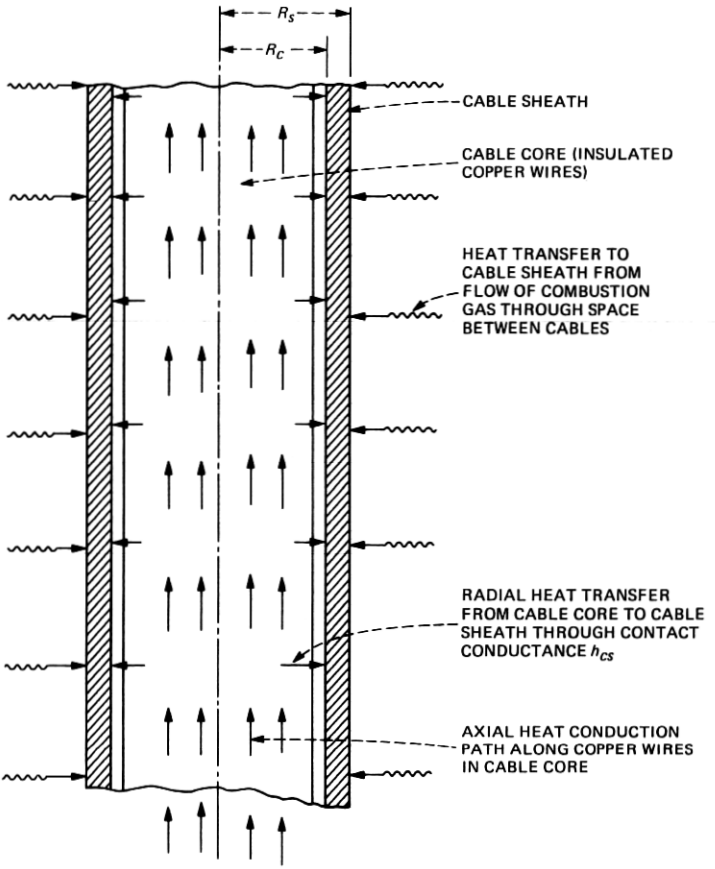

Fig. 2—Heat transfer modes in firestopped cables.

the limit, to an approximate continuum representation of heat conduction in the cable core. This development follows.

Consider the individual conductor wires as composite cylinders with copper wire radius r_c (see the appendix for a list of parameters) on which is affixed an insulating material with thickness $(r_d - r_c)$, as shown in Fig. 3. When radial symmetry prevails, Fourier heat conduction equations and boundary conditions for the conductor wire assume the following forms:

$$k_{cu}\left[\frac{\partial^2 T_{cu}}{\partial z^2}+\frac{1}{r}\frac{\partial}{\partial r}\left(r\frac{\partial T_{cu}}{\partial r}\right)\right]=(\rho c)_{cu}\frac{\partial T_{cu}}{\partial t}, \qquad \begin{matrix} z>0 \\ 0\le r\le r_c, \\ t>0 \end{matrix} \qquad (1)$$

for the copper wire conductors, and

$$k_i\left[\frac{\partial^2 T_i}{\partial z^2}+\frac{1}{r}\frac{\partial}{\partial r}\left(r\frac{\partial T_i}{\partial r}\right)\right]=(\rho c)_i\frac{\partial T_i}{\partial t}, \qquad \begin{matrix} z>0 \\ r_c\le r\le r_d, \\ t>0 \end{matrix} \qquad (2)$$

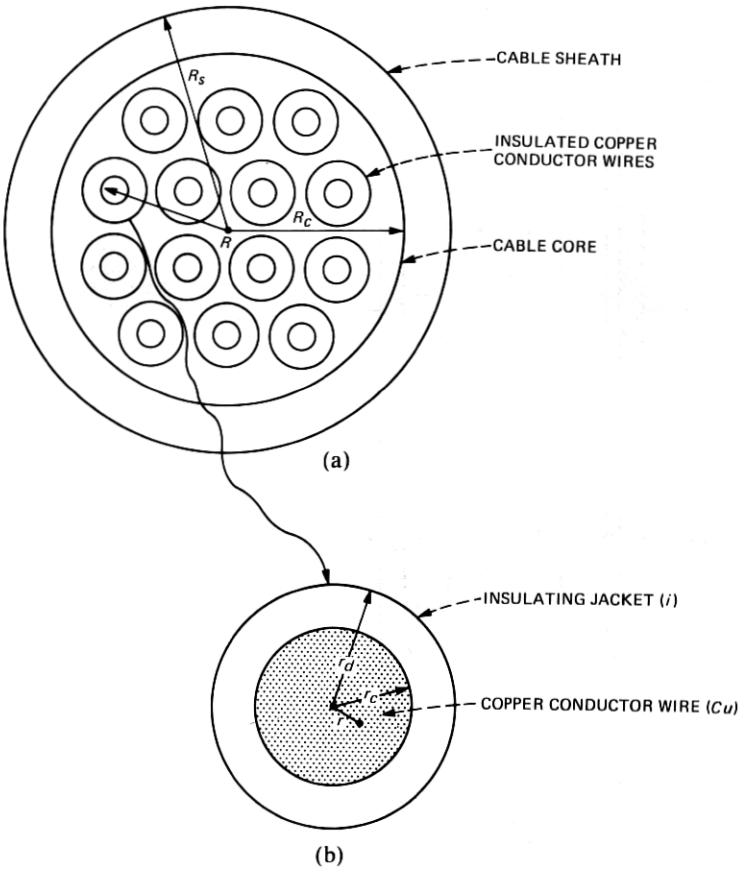

Fig. 3—(a) Macrocoordinate and (b) microcoordinate systems.

for the insulation, with boundary conditions:

$$T_{cu}(0, z, t) = \text{finite}, \tag{3}$$

$$T_{cu}(r_c, z, t) = T_i(r_c, z, t),^* \tag{4}$$

$$k_{cu} \frac{\partial T_{cu}}{\partial r}(r_c, z, t) = k_i \frac{\partial T_i}{\partial r}(r_c, z, t), \tag{5}$$

$$k_i \frac{\partial T_i}{\partial r}(r_d, z, t) = -h_i[T_i(r_d, z, t) - \hat{T}(z, t)], \tag{6}$$

and initial conditions:

$$T_{cu}(r, z, 0) = T_i(r, z, 0) = 0. \tag{7}$$

* A perfect contact between the copper wire and insulation is assumed, since the insulation is literally molded onto the wire.

In the above equations, $T(r, z, t)$ is the temperature, k is the thermal conductivity, ρc is the volumetric sensible heat capacity, z is the axial coordinate along the length of wire, r is the radial coordinate, t is the time, h_i is an effective linear heat transfer coefficient, and $\hat{T}(z, t)$ is a temperature to be assigned subsequently. The subscripts "cu" and "i" are assigned to quantities associated with the copper conductor and insulation, respectively. Since the diameter of the wire is much smaller than its length, it is convenient to express the temperature in the series

$$T_{cu}(r, z, t) = T_o(z, t) + T_{cu}^{(1)}(r, z, t) + \cdots, \tag{8}$$

and

$$T_i(r, z, t) = T_o(z, t) + T_i^{(1)}(r, z, t) + \cdots. \tag{9}$$

The leading term in eqs. (8) and (9) is the average temperature, i.e.,

$$T_o(z, t) = \frac{2}{r_d^2}\left[\int_0^{r_c} rT_{cu}(r, z, t)dr + \int_{r_c}^{r_d} rT_i(r, z, t)dr\right], \tag{10}$$

from which it follows that

$$\int_0^{r_c} rT_{cu}^{(n)}(r, z, t)dr + \int_{r_c}^{r_d} rT_i^{(n)}(r, z, t)dr = 0,$$

$$n = 1, 2, 3, \cdots. \tag{11}$$

Substituting series (8) and (9) into differential equations (1) and (2) produces a set of recurrent differential equations:

$$k_{cu}\left[\frac{\partial^2 T_{cu}^{(n-1)}}{\partial z^2} + \frac{1}{r}\frac{\partial}{\partial r}\left(r\frac{\partial T_{cu}^{(n)}}{\partial r}\right)\right] = (\rho c)_{cu}\frac{\partial T_{cu}^{(n-1)}}{\partial t},$$

$$n = 1, 2, \cdots \tag{12}$$

$$k_i\left[\frac{\partial^2 T_i^{(n-1)}}{\partial z^2} + \frac{1}{r}\frac{\partial}{\partial r}\left(r\frac{\partial T_i^{(n)}}{\partial r}\right)\right] = (\rho c)_i\frac{\partial T_i^{(n-1)}}{\partial t}.$$

$$n = 1, 2, \cdots. \tag{13}$$

All $T_{cu}^{(n)}(r, z, t)$ and $T_i^{(n)}(r, z, t) n = 1, 2, 3, \cdots$ are then expressible in terms of the average temperature, $T_o(z, t)$. Retaining terms up to first order, it follows from (12) and (13) that

$$T_{cu}(r, z, t) = T_o(z, t) - \frac{r^2}{4k_{cu}}L^{cu} + A(z, t)\ln r + B(z, t), \tag{14}$$

and

$$T_i(r, z, t) = T_o(z, t) - \frac{r^2}{4k_i}L^i + C(z, t)\ln r + D(z, t), \tag{15}$$

where

$$L^{cu} = k_{cu}\frac{\partial^2 T_o}{\partial z^2} - (\rho c)_{cu}\frac{\partial T_o}{\partial t},\ L^i = k_i\frac{\partial^2 T_o}{\partial z^2} - (\rho c)_i\frac{\partial T_o}{\partial t}.$$

The variables of integration A, B, C, D are determined from boundary conditions, eqs. (3) through (5) and eq. (11). The final form of the temperature in the copper wire and insulation in terms of the average temperature $T_o(z, t)$ is

$$T_{cu}(r, z, t) = T_o(z, t) + \frac{1}{4k_{cu}}\left(r_c^2 - \frac{r_c^4}{2r_d^2} - r^2\right)L^{cu} + \frac{r_c^2}{2k_i}\ln(r_d/r_c)(L^{cu} - L^i) + \frac{(r_d^2 - r_c^2)}{4k_i r_d^2}\left[-r_c^2 L^{cu} + \frac{(r_d^2 + r_c^2)}{2}L^i\right], \quad (16)$$

and

$$T_i(r, z, t) = T_o(z, t) + \frac{1}{k_i}\left(\frac{r_d^4 - r_c^4}{8r_d^2} + \frac{r_c^4}{4} - \frac{r^2}{4}\right)L^i + \frac{r_c^2\ln(r/r_d)}{2k_i}(L^i - L^{cu}) - \left[\frac{r_c^2}{4k_i r_d^2}(r_d^2 - r_c^2) + \frac{r_c^4}{8k_{cu}r_d^2}\right]L^{cu}. \quad (17)$$

It now remains to obtain the differential equation for the average temperature, $T_o((z, t)$. This equation comes from the satisfaction of the boundary condition at $r = r_d$, as shown in eq. (6);

$$\left[\frac{1}{2} - \frac{r_c^2}{2r_d^2} + \frac{h_i}{8r_d^3 k_i}(r_d^2 - r_c^2)^2\right]L^i + \left\{\frac{r_c^2}{2r_d^2} + \frac{h_i}{8r_d^3}\left[\frac{2r_c^2(r_d^2 - r_c^2)}{k_i} + \frac{r_c^4}{k_{cu}}\right]\right\}L^{cu} = \frac{h_i}{r_d}[T_o(z, t) - \hat{T}(z, t)]. \quad (18)$$

Relating the variables in each conductor wire to those of neighboring ones in the limit leads to a continuum base from a discrete one. To arrive at this continuum description of the cable core consider the wires as embedded in a radially symmetric macrocoordinate system, as shown in Fig. 3. The center of, say, the nth conductor is located at R_n and eq. (18) is written at this point. In keeping with the assumption of radial symmetry, the temperature on the right of (18), $\hat{T}(z, t)$, is related to the average temperature of adjacent wires $T_o^{(n+1)}$ and $T_o^{(n-1)}$ located at $R_n + 2r_d$ and $R_n - 2r_d$, respectively. To determine $\hat{T}(z, t)$ the temperatures are weighted with respect to the location of the wire in the cable core. This has the effect of enforcing radial symmetry

$$\hat{T}(z, t) = \frac{1}{2R_n}[(R_n + r_d)T_o^{(n+1)} + (R_n - r_d)T_o^{(n-1)}]. \quad (19)$$

Thus, if D is used to denote the difference appearing on the right of (18), it can be written with the aid of (19) as

$$D = -\frac{1}{2R_n}[(R_n + r_d)T_o^{(n+1)} - 2R_nT_o^{(n)} + (R_n - r_d)T_o^{(n-1)}]. \quad (20)$$

When we expand $T_o^{(n+1)}$ and $T_o^{(n-1)}$ in a Taylor series about R_n, eq. (20) becomes

$$D = -\frac{2(r_d)^2}{R_n}\left\{\frac{\partial}{\partial R_n}\left[R_n\frac{\partial T_o^{(n)}}{\partial R_n}\right] + 0(r_d)\right\}. \quad (21)$$

If we substitute (21) into (18) and consider $r_d \ll 1$ so that only the first term on the right of (21) is significant, the final form of the continuum representation of the cable core, after the subscript n is eliminated, is obtained as:

$$\left[1 - \frac{r_c^2}{r_d^2} + \frac{h_i(r_d^2 - r_c^2)^2}{4r_d^3k_i}\right]L^i + \left\{\frac{r_c^2}{r_d^2} + \frac{h_i}{4r_d^3}\left[\frac{2r_c^2(r_d^2 - r_c^2)}{k_i} + \frac{r_c^4}{k_{cu}}\right]\right\}L^{cu} + \frac{4h_ir_d}{R}\frac{\partial}{\partial R}\left(R\frac{\partial T_o}{\partial R}\right) = 0. \quad (22)$$

The quantity $(4h_ir_d)$ has the dimensions of conductivity and represents the effective radial conductivity of the cable core. The conductivity in the axial direction reflects the effect of the microstructure and is given as

$$(k_z)_{\text{eff.}} = \left[1 - \frac{r_c^2}{r_d^2} + \frac{h_i(r_d^2 - r_c^2)^2}{4r_d^3k_i}\right]k_i + \left\{\frac{r_c^2}{r_d^2} + \frac{h_i}{4r_d^3}\left[\frac{2r_c^2(r_d^2 - r_c^2)}{k_i} + \frac{r_c^4}{k_{cu}}\right]\right\}k_{cu}, \quad (23a)$$

and the effective heat capacity as

$$(\rho c)_{\text{eff.}} = \left[1 - \frac{r_c^2}{r_d^2} + \frac{h_i(r_d^2 - r_c^2)^2}{4r_d^3k_i}\right](\rho c)_i + \left\{\frac{r_c^2}{r_d^2} + \frac{h_i}{4r_d^3}\left[\frac{2r_c^2}{k_i}(r_d^2 - r_c^2) + \frac{r_c^4}{k_{cu}}\right]\right\}(\rho c)_{cu}. \quad (23b)$$

Notice that when the conductor wires are assumed insulated, i.e., $h_i = 0$, there is no radial heat flow and the effective heat capacity and axial conductivity are given, as expected, by the law of mixtures.

Now that the heat conduction equation for the cable core has been determined, it remains to obtain the equation that governs the heat transfer in the entire cable including the outer sheath. This development parallels the procedure employed above. The only exception is that, since the cable core and sheath are not generally in perfect contact, the average temperatures in the cable core and sheath are assumed to be different. In many cables the cable core can be pushed

through the cable sheath with only a moderate pressure. Since the axial conductivity of the cable core is much larger than that of the cable sheath, as a simplification, it appears reasonable to assume that the axial heat conduction in the cable sheath can be neglected. Thus, the expression for the temperature in the cable core and sheath assumes the form

$$T_o(R, z, t) = T_o^{(0)}(z, t) + \frac{(2R^2 - R_c^2)}{8k_R^{(c)}} L^{(0)}(z, t), \qquad 0 \le R \le R_c \quad (24a)$$

and

$$T_s(R, z, t) = T_s^{(0)}(z, t) + \frac{1}{4\kappa_s}\left[R^2 - \frac{(R_s^2 + R_c^2)}{2}\right]\frac{\partial T_s^{(0)}}{\partial t}(z, t)$$
$$+ \frac{R_c^2}{2}\left[\ln(R/R_c) - \frac{R_s^2}{R_s^2 - R_c^2}\ln(R_s/R_c) + \frac{1}{2}\right]\left[L^{(0)}(z, t) - \frac{1}{\kappa_s}\frac{\partial T_s^{(0)}}{\partial t}\right],$$
$$R_c \le R \le R_s, \quad (24b)$$

where

$$L^{(0)}(z, t) = (\rho c)_{\text{eff}}\frac{\partial T_0^{(0)}}{\partial t} - (k_z)_{\text{eff}}\frac{\partial^2 T_0^{(0)}}{\partial z^2}$$

and $T_o^{(0)}(z, t)$, $T_s^{(0)}(z, t)$ are the average cable core and cable sheath temperatures, respectively. The other parameters are defined in the appendix. The average cable core and cable sheath temperatures given above are related through the imperfect heat transfer boundary condition at $R = R_c$, namely,

$$k_R^{(c)}\frac{\partial T_o}{\partial R} = -h_{cs}(T_o - T_s)\big|_{R=R_c}. \quad (25)$$

It follows that

$$\left\{\frac{R_c}{2} + \frac{h_{cs}R_c^2}{8k_R^{(c)}} - \frac{h_{cs}R_c^2}{2k_s}\right.$$
$$\left.\cdot\left[\frac{-R_s^2}{R_s^2 - R_c^2}\ln(R_s/R_c) + \frac{1}{2}\right]\right\}L^{(0)}(z, t) + h_{cs}T_o^{(0)}(z, t)$$
$$= \left\{\frac{h_{cs}(R_c^2 - R_s^2)}{8\kappa_s} - \frac{h_{cs}R_c^2}{2\kappa_s}\left[-\frac{R_s^2\ln(R_s/R_c)}{R_s^2 - R_c^2} + \frac{1}{2}\right]\right\}$$
$$\cdot\frac{\partial T_s^{(0)}}{\partial t}(z, t) + h_{cs}T_s^{(0)}(z, t), \quad (26)$$

where h_{cs} is the heat transfer coefficient between the cable core and cable sheath.

In the following section eqs. (24b) and (26) are used to determine

the heat transfer in an array of sheathed cables that form a bundle. However, before this is accomplished it is worthwhile to briefly summarize the preceding developments.

The cable core is obviously not a continuum; consequently, a microstructural characterization starting with an individual conductor wire was used to derive the governing radially symmetric heat conduction equation for the cable core. This derivation produces an effective or averaged macroscopic continuum representation of the cable core that retains the physical characteristics of the conductor wire microstructure. It is, however, anisotropic, since the thermal conductivity in the axial and radial directions is not equal. After we obtain the governing equations for heat flow in the core, the equations that the cable sheath temperature satisfies [eqs. (24b) and (26)] were then determined. These were obtained, paralleling the preceding microstructural derivation, for heat flow predominantly in the axial direction. The radial heat transfer is introduced as a perturbation.

III. HEAT TRANSFER THROUGH A CABLE BUNDLE

The objective of this investigation is to analyze heat flow through firestopped cable bundles during fire tests. The ASTM E119 temperature-time history, Fig. 1, provides the fire environment. A typical firestopped cable bundle configuration and the above- and below-floor coordinate system is illustrated in Fig. 4.

As previously mentioned, cable penetrations vary in size and in the number and type of cables accommodated; to lend a degree of definiteness to the analysis it is convenient to consider a widely used arrangement. A square cable array containing nine cables, as illustrated in Fig. 5, is a mathematically manageable configuration, yet most of the heat transfer characteristics of larger cable arrays are maintained. From the point of view of symmetry, only three cables need be considered—the corner cable, to be designated hereafter as cable 1, the side cable, to be denoted as cable 2, and the center cable, to be called cable 3.

The section of each cable below the slab (see Fig. 4) is directly exposed in a furnace to a fire temperature of up to 1000 degrees centigrade and, therefore, after only a short time all polymeric insulating material is burned away. In the model this effect is approximated by assuming that only a loose array of independent copper wires projects below the slab. This section of the cable bundle extending up through and above the floor slab experiences a different thermal environment. A zone of decomposition of the polymetric insulating materials occurs and creeps upwards during the extended period of exposure to the below-floor fire. This zone of charred and expanded insulating material alters the temperature in the void spaces. In the

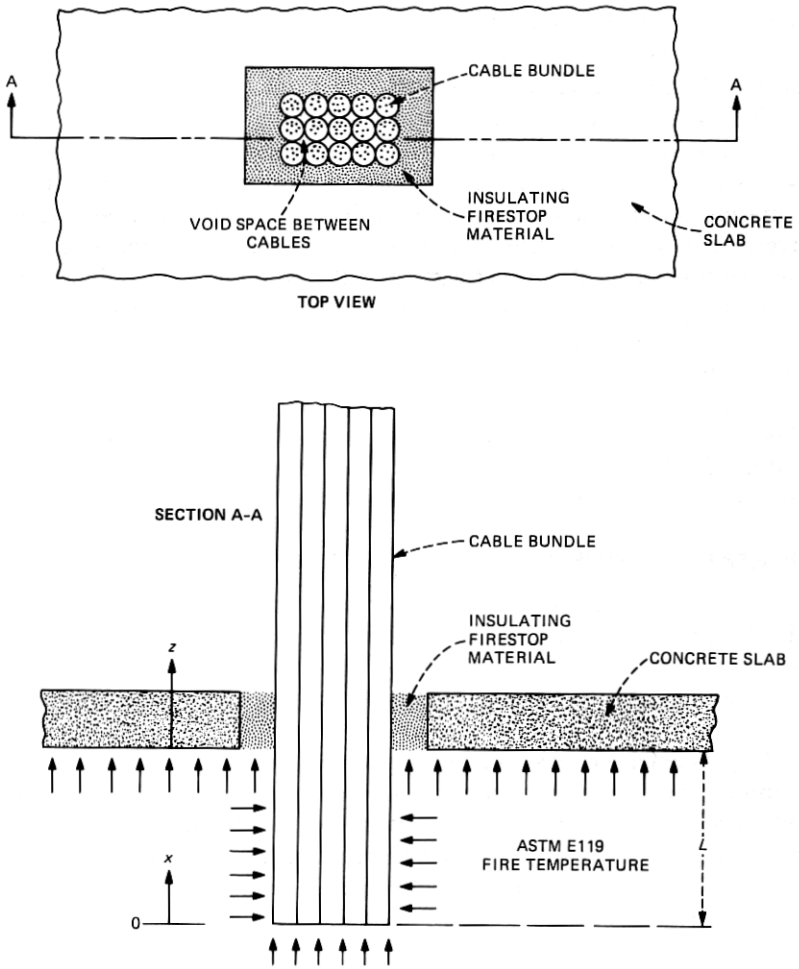

Fig. 4—Typical cable opening firestop test configuration.

present analysis the effect of this nonlinear phenomenon is ignored to render the analysis tractable. It is conservatively assumed here that the hot furnace gases move unimpeded in the void space between cables.

The average cable core and average cable sheath temperature for each of three cables is determined by performing a heat balance at the outer cable sheath surface $R = R_s$. This leads to the following three coupled equations:

$$k_s \frac{\partial T_s^{(1)}}{\partial R}(R_s, z, t) = 2A_c H_{cB}[T_s^{(2)} - T_s^{(1)}] + (3A_f + 2A_c)H_f[T_f^{(0)} - T_s^{(1)}]$$

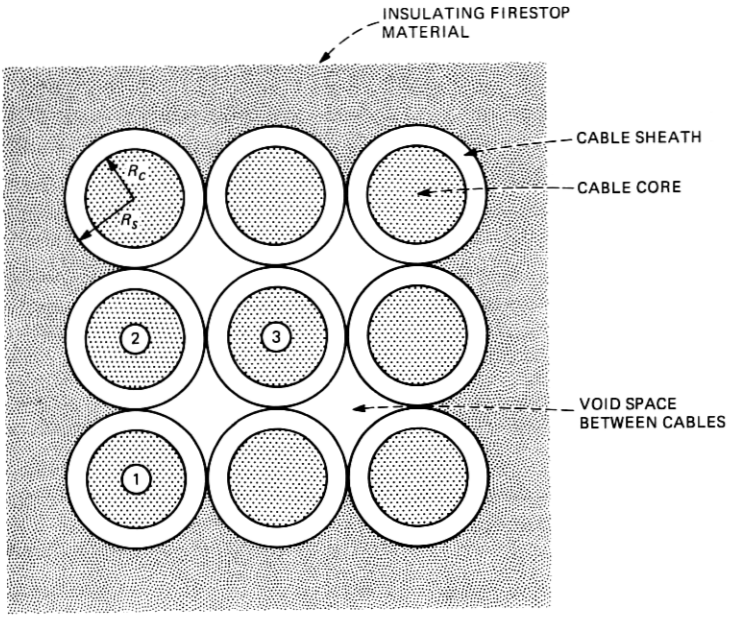

Fig. 5—Cable bundle configuration considered.

$$+ A_f H_1[T_f^{(1)} - T_s^{(1)}] + 2A_f H_r F_{12}[T_s^{(2)} - T_s^{(1)}] + A_f H_r F_{22}[T_s^{(3)} - T_s^{(1)}]|_{R=R_s} \quad (27a)$$

$$k_s \frac{\partial T_s^{(2)}}{\partial R}(R_s, z, t) = 2A_c H_{cB}[T_s^{(1)} - T_s^{(2)}] + (A_c H_{cB} + 2A_f H_r F_{12}) \cdot [T_s^{(3)} - T_s^{(2)}] + 2A_f H_1[T_f^{(2)} - T_s^{(2)}] + (2A_f + A_c)H_f[T_f^{(0)} - T_s^{(2)}] + 2A_f H_r F_{12}[T_s^{(1)} - T_s^{(2)}]|_{R=R_s} \quad (27b)$$

$$k_s \frac{\partial T_s^{(3)}}{\partial R}(R_s, z, t) = 4A_c H_{cB}[T_s^{(2)} - T_s^{(3)}] + 4A_f H_1[T_f^{(1)} - T_s^{(3)}] + 8A_f H_r F_{12}[T_s^{(2)} - T_s^{(3)}] + 4A_f H_r F_{22}[T_s^{(1)} - T_s^{(3)}]|_{R=R_s}. \quad (27c)$$

In the above equations the parameter A_c denotes the fraction of the cable sheath perimeter that is in contact with an adjacent cable, and A_f the portion exposed to the hot furnace gases that flow up through the interstices of the cable. It therefore follows that $4(A_c + A_f) = 1$. H_{cB} is the solid-contact conductance between the cables, H_f is the heat transfer coefficient between the cables and the firestop material, H_1 is the convective heat transfer coefficient between the cable and the hot furnace gases that flow up through the void spaces between cables,

and H_r is a linearized black body radiative heat transfer coefficient between the cables. F_{12} and F_{22} are radiation form factors between cable 3 and cable 2, and cable 1 and cable 3, respectively. The temperatures $T_f^{(0)}(z, t)$ and $T_f^{(1)}(z, t)$ are assumed known and represent the temperature distribution in the mineral wool insulating firestop material surrounding the cable bundle and the temperature of the furnace gases that move up through the void spaces between cables, respectively.

At this juncture, it is convenient to eliminate the independent time variable t from the equations by introducing the Laplace transformation

$$\bar{T}(z; p) = \int_0^\infty T(z, t)e^{-pt}\, dt. \tag{28}$$

In what follows, a bar over a variable indicates that the transformation (28) has been performed. Substituting eq. (24b) into (27) and using eq. (26) to eliminate the average cable sheath temperature, we produce a system of three coupled ordinary differential equations for the transformed average cable core temperatures $\bar{T}_{0,1}^{(0)}$, $\bar{T}_{0,2}^{(0)}$, and $\bar{T}_{0,3}^{(0)}$:

$$\begin{aligned}
&(\Gamma_1 D^2 - \Delta_1)\bar{T}_{0,1}^{(0)} - 2(\gamma_1 D^2 - \theta_1)\bar{T}_{0,2}^{(0)} - (\eta_1 D^2 - \epsilon_1)\bar{T}_{0,3}^{(0)} \\
&= -(h_{cs} + pE_1)[(3A_f + 2A_c)H_f\bar{T}_f^{(0)} + A_f H_1 \bar{T}_f^{(1)}], \qquad (29a) \\
&-2(\gamma_1 D^2 - \theta_1)\bar{T}_{0,1}^{(0)} + (\Gamma_2 D^2 - \Delta_2)\bar{T}_{0,2}^{(0)} - (\eta_2 D^2 - \epsilon_2)\bar{T}_{0,3}^{(0)} \\
&= -(h_{cs} + pE_1)[(2A_f + A_c)H_f\bar{T}_f^{(0)} + 2A_f H_1 \bar{T}_f^{(1)}], \qquad (29b) \\
&-4(\eta_1 D^2 - \epsilon_1)\bar{T}_{0,1}^{(0)} - (\gamma_3 D^2 - \theta_3)\bar{T}_{0,2}^{(0)} + (\Gamma_3 D^2 - \Delta_3)\bar{T}_{0,3}^{(0)} \\
&= -4(h_{cs} + pE_1)A_f H_1 \bar{T}_f^{(1)}, \qquad (29c)
\end{aligned}$$

where the operator $D^2 = \dfrac{d^2}{dz^2}$ and the coefficients Γ, Δ, γ, θ, η, and ϵ are linear functions of the transform parameter p. After considerable algebra the system of differential equations (29) is solved for the three average cable core temperatures in the form

$$\begin{aligned}
\bar{T}_0^{(0)} = C_1\exp(-z\sqrt{m_1}) + C_2\exp(-z\sqrt{m_2}) + C_3\exp(-z\sqrt{m_3}) \\
-(h_{cs} + pE_1)[R\bar{T}_f^{(0)} + H\bar{T}_f^{(1)}]. \qquad (30)
\end{aligned}$$

The quantities m_1, m_2, and m_3 are functions of the Laplace transform parameter p and are evaluated as the roots of the characteristic cubic equation of the system of equations in (29). The coefficients of integration C_1, C_2, and C_3 are determined by matching the solution of the cable section below the slab. This is accomplished by enforcing tem-

perature and energy continuity for each of the three cables at the common boundary $Z = 0$ and $X = L$, as shown in Fig. 4. The cable sheath temperature evaluated at $R = R_s$ follows from (30) in the form

$$\bar{T}_s(R_s, z, p) = \left[\frac{h_{cs} + pB_1}{h_{cs} + pE_1}(1 + pA_1) + pD_1\right]\bar{T}_0^{(0)} - (\kappa_z)_{\text{eff}}\left[\frac{B_1(1 + pA_1)}{(h_{cs} + pE_1)} + D_1\right]\frac{d^2\bar{T}_0^{(0)}}{dz^2}, \quad (31)$$

where A_1, B_1, D_1 and E_1 are constants.

The temperatures presented in this section are in the Laplace transform domain and must be inverted to the real-time regime. The functions, however, are too complicated to be inverted in closed form. A numerical procedure using the method of quadratures to obtain these inversions is discussed in Section IV.

IV. INVERSION OF LAPLACE TRANSFORM TEMPERATURE SOLUTION

The form of the transformed temperature solution given in eqs. (30) and (31) is much too complicated to use for obtaining a closed-form inversion formula. Consequently, we must resort to a numerical inversion procedure. Most of the methods that appear in the literature involve expanding the transformed function in a series that could then be inverted term by term using tabulated formulae. Littlewood and Zakian[1] suggest expanding in a series of Chebyshev polynomials, while Longman[2] proposes using the Pade table for the Taylor series expansion of the transformed function. Both of these methods were judged to be impractical because of the complexity of the functions to be inverted here.

The method that was finally adopted was developed by Talbot.[3] The inversion of arbitrary transforms is accomplished by a method of quadrature along a special contour in the complex plane. The standard inversion formula for a transformed function $\bar{F}(p)$ involves performing the following integration in the complex plane:

$$F(t) = \frac{1}{2\pi i}\int_{\gamma - i\infty}^{\gamma + i\infty} \bar{F}(p)e^{pt}dp, \quad (32)$$

where p is considered a complex variable, $i = (-1)^{1/2}$, and γ is to the right of all the singularities of $\bar{F}(p)$. In Talbot's method the path of integration indicated by (32) is deformed to the path L shown in Fig. 6, the equation of which is

$$p = \alpha + i\theta, \quad (33)$$

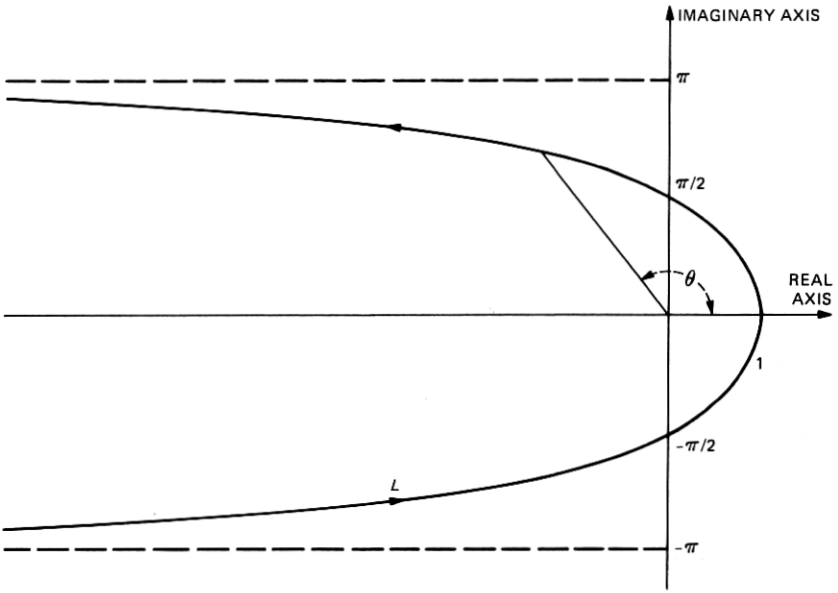

Fig. 6—Path L for Laplace transform inversion.

where $\alpha = \theta \cot \theta$.

Path L is equivalent to the standard integration path providing that

(i) L encloses all singularities of $\bar{F}(p)$, and

(ii) $|\bar{F}(p)| \to 0$ uniformly in $Re\, p \leq 0$ as $|p| \to \infty$.

Condition (ii) holds for the functions considered here. Condition (i), in general, may not be satisfied by a given $\bar{F}(p)$; however, the modified function $\bar{F}(\lambda p + \sigma)$ for suitable scaling and shift factors λ and σ can be made to conform. In this regard, for the functions to be inverted here it can be argued that the singularities exhibited by eqs. (30) and (31) are located on the negative real axis; consequently, condition (i) is satisfied without resorting to scaling or shift factors. However, to accurately perform the inversions over large intervals of time (the temperatures are calculated for times up to two hours) a scaling factor $\lambda > 1$ is necessary. This scaling factor merely shifts the singularity along the negative real axis closer to the origin.

Once conditions (i) and (ii) are satisfied, the inversion formula (32), when taken about L assumes the form

$$F(t) = \frac{\lambda e^{\sigma\tau}}{2\pi i} \int_{-\pi}^{\pi} e^{p\tau} \bar{F}(\lambda p + \sigma) \frac{dp}{d\theta}\, d\theta, \qquad \tau = \lambda t. \tag{34}$$

Finally, "⅓" Simpson quadrature with equal intervals π/n in the variable θ gives the approximation

$$F(t) \sim \frac{\lambda e^{\sigma\tau}}{3n} \{Re(H_0 + 4H_1 + 2H_2 + 4H_3 + \cdots + 4H_{n-1})\}, \quad (35)$$

where

$$H_k = H(p)|_{\theta_k},$$

$$\theta_k = k\pi/n \qquad (k = 0, \cdots, n-1)$$

$$H(p) = e^{p\tau}\bar{F}(\lambda p + \sigma)(1 + i\beta),$$

and

$$\beta = [\theta - \tfrac{1}{2}\sin(2\theta)]/\sin^2\theta.$$

The symbol Re indicates that only the real part of the complex quantity is taken. Sufficient accuracy is obtained by a suitable choice of n, λ, and σ. The principles of choice are presented by Talbot[3] and will not be discussed here.

A check of this technique was made by inverting the function given in Ref. 2. In all instances satisfactory results were obtained. For numerical inversions performed here, it was found sufficient to take $n = 20$, $\lambda = 8$, and $\sigma = 0$.

V. DISCUSSION AND SUMMARY

The concept of firestopping any type of penetration is synonymous with retarding the flow of heat from the fire side of the penetration to the unexposed side. The problem rests solely on the identification of procedures and materials to seal the space adjacent to the penetrant to meet certain standards. Cables by their very nature have excellent thermal conduction properties in the longitudinal direction. Very little can be done to prevent heat conduction up the array of copper wire conductors that make up the center core section of the cable. However, it appears reasonable to measure the efficiency of a firestop by the temperature rise on the free surfaces on the unexposed side of the penetration. If these surfaces are maintained at sufficiently low temperatures, ignition of combustibles that happen to be in direct contact or in close proximity cannot occur. In the case of cable penetrations the critical surfaces are the horizontal firestopping material surface on the unexposed side and the vertical cable sheath surfaces at the outer perimeter of the cable bundle, as shown in Fig. 4. In normal practice the firestop material is chosen to be a good thermal insulator and is applied with sufficient depth to preclude high temperatures at the top surface. Thus, the efficiency of the firestopped geometry will, in general, be determined more by the temperature rise on the cable sheath surface of the outer perimeter cables than by the firestop material. To ascertain the temperature at this critical location, a

theoretical transient heat transfer model of a firestopped cable bundle was developed. In addition to heat flow through the cable core, the model treats the lateral heat flow from the cable core to the cable sheath and convective heat transfer to the cable sheath from the flow of combustion gases through the interstices between the cables. The standard ASTM E119 temperature variation is applied at one end of the cable bundle and the temperature distribution of the individual cables is computed along the length for up to two hours. To quantify these effects, temperature distribution was computed at 10-minute intervals for two hours at the 20-cm and 30-cm firestopped depth for three different cable types—switchboard, terminating, and power cable. For each of these cable types the following parameters were varied:

(*i*) R_s, cable radius

(*ii*) A_c, fraction of cable sheath surface in contact with an adjacent cable

(*iii*) h_{cs}, conductance between cable core and sheath

(*iv*) H_f, conductance between cable bundle perimeter and firestop material

(*v*) Δp, furnace pressure.

Some remarks concerning the inclusion of the furnace pressure as a parameter are in order. Furnace pressure influences the magnitude of the heat transmitted to the cable sheath—by the hot furnace gases that travel up through the space between cables—through the heat transfer coefficient H_1, as shown in eq. (27). The value of H_1 is computed from standard empirical formulae[4] once the gas flow velocity and flow-channel characteristics are known. The steady-state gas velocity is calculated from the furnace pressure assuming that the spaces between cables are independent flow channels.[5] In general, H_1 increases with increased furnace gas pressure.

Some of the results of the analysis for a given type cable are given in Table I and Fig. 7. The calculated end-point temperature at $z = 30$ cm in Fig. 6 and $t = 2$ hours for the cable sheath and core are given in Table I, and a typical temporal temperature distribution is given in Fig. 7. The temperatures given in Table I and Fig. 7 should not be construed to be indicative of actual measured test values. As previously indicated, the model does not take into account nonlinear aspects of this obviously complex phenomenon, such as potential combustion modes and melting of the polymeric materials that in some instances could conceivably, for periods of time, constrict the void of spaces between cables and thereby reduce the flow of furnace gases. Nevertheless, the sensitivity of the cable temperatures to changes in the linear cable bundle parameters identified in the model, H_f, A_c, R_s, and Δp can be calculated and are presented in Table I.

Table I—Calculated temperatures at $z = 30$ cm and $t = 2$ hours for various values of the cable bundle parameters

Case	H_f (W/cm^2—°C)	A_c	R_s (cm)	Δp (cm of Water)	Cable Sheath Temperature (°C) Rise		Cable Core Temperature (°C) Rise	
					Cable 1	Cable 3	Cable 1	Cable 3
1	0.034	0.1	1.27	1	115	164	199	246
2	0.017	0.1	1.27	1	224	265	293	332
3	0.017	0.15	1.27	1	170	190	248	270
4	0.017	0.1	0.635	1	93	115	135	154
5	0.017	0.1	1.27	0.13	102	115	188	204

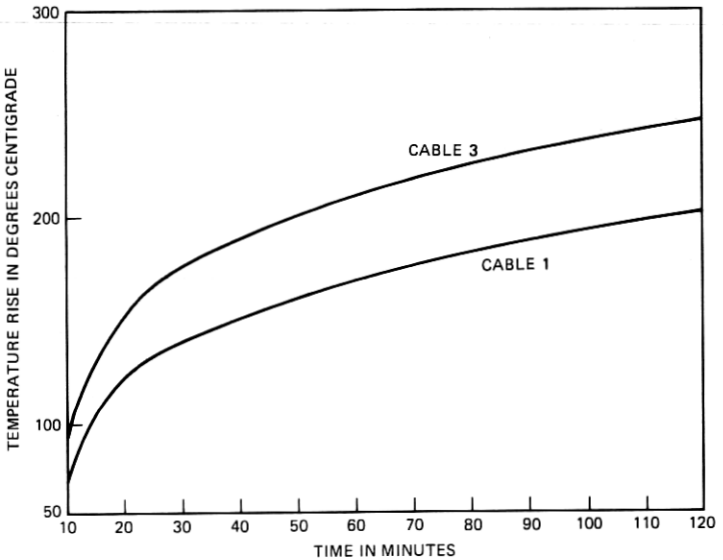

Fig. 7—Cable core temperature for Case 1 cable bundle parameters given in Table I.

It is clearly shown in Table I that the cable core temperature exceeds that of the cable sheath. A tightly packed firestop that exerts lateral pressure on the side of the cable array will provide sufficient heat sinking to reduce the temperature in the cable bundle. This physical effect is embodied in the contact conductance parameter, H_f. The larger the numerical value of this parameter, the tighter the firestop packing. Cases 1 and 2 of Table I show that increasing this parameter indeed results in a lowering of the cable sheath and cable core temperatures.

The same general result prevails when furnace overpressure Δp is reduced. This effectively reduces the heat transfer coefficient H_1 between the cable sheath and the hot furnace gases. This is demonstrated in Table I by comparing the end-point cable temperatures of

Cases 2 and 5. Cable temperature can also be reduced by increasing the contact surface between cables, as measured by an increase in the parameter A_c, suggesting a tighter and more compact cable bundle. The cable temperatures, as observed in Cases 2 and 3, are also lowered. This is primarily due to the resulting smaller void space between the cables and secondarily to the larger conduction path presented to the interior cables.

VI. CONCLUSIONS

The following trends were generally indicated:

(*i*) The cable core and cable sheath temperature is largest for the interior cable (cable 3 of Fig. 5) and the smallest for the corner cable (cable 1 of Fig. 5).

(*ii*) The temperature of cable core exceeds that of the cable sheath.

(*iii*) The primary heat transfer mode to the cable sheath is from the flow of hot combustion gases through the void space between cables.

(*iv*) Reducing the void space between the cables by tightly packing the cables and/or using smaller diameter cables impedes the flow of hot combustion gases and results in a significant reduction of the primary convective heat transmission mode.

(*v*) A tightly packed firestop capable of providing some heat sinking to the cooler environs is the most practical and effective method of reducing the heat transfer properties of the cable bundle.

(*vi*) The magnitude of the cable sheath temperature for similar size cables depends on the furnace gas pressure and, to a lesser degree, on the firestop depth.

VII. ACKNOWLEDGMENT

The comments and suggestions made by J. Simpson in the preparation of the text are appreciated. In addition, appreciation is expressed to W. Pferd for reviewing several drafts of the manuscript and suggesting valuable comments for its improvement.

REFERENCES

1. R. K. Littlewood and V. Zakian, "Numerical Evaluation of Fourier Integrals," J. Inst. Maths. Applics., *18* (December 1976), pp. 333–9.
2. I. M. Longman, "Numerical Laplace Transform Inversion of a Function Arising in Viscoelasticity," J. Comp. Phys., *10* (December 1972), pp. 224–31.
3. A. Talbot, "A New Method for Numerical Inversion of Laplace Transforms," IEEE Proc., *ISCAS* (1976), pp. 130–3.
4. C. P. Kothandaraman and S. Subramanyan, *Heat and Mass Transfer Data Book*, New York: Halsted Press, 3rd edition, 1977.
5. R. G. Binder, *Fluid Mechanics*, Englewood Cliffs, N.J.: Prentice-Hall, 3rd edition, 1955.

A_c—Fraction of cable sheath surface in contact with an adjacent cable.

A_f—Fraction of cable surface in contact with combustion gases, $4(A_c + A_f) = 1$.

F_{12}, F_{22}—Radiation form factors between cables.

H_1—Heat transfer coefficient between cable and combustion gases.

H_{cB}—Solid contact conductance between cables.

H_f—Contact conductance between cable bundle perimeter and firestop.

H_r—Linearized black body radiative heat transfer coefficient.

h_{cs}—Conductance between cable core and cable sheath.

h_i—Conductance between individual copper conductor wires.

$k_R^{(c)} = 4h_i r_d$—Effective radial thermal conductivity of cable core.

k_{cu}—Thermal conductivity of copper wire.

k_i—Thermal conductivity of wire insulation.

k_s—Thermal conductivity of cable sheath.

$(k_z)_{\text{eff}}$—Effective axial thermal conductivity of cable core.

$\kappa_{cu} = k_{cu}/(\rho c)_{cu}$—Thermal diffusivity of copper wire.

$\kappa_i = k_i/(\rho c)_i$—Thermal diffusivity of wire insulation.

$\kappa_s = k_s/(\rho c)_x$—Thermal diffusivity of cable sheath.

$(\kappa_z)_{\text{eff}} = (k_z)_{\text{eff}}/(\rho c)_{\text{eff}}$—Effective axial thermal diffusivity of cable core.

L—Length of cable below slab.

R_c—Radius of cable core.

R_s—Overall radius of cable.

r_c—Radius of single copper conductor wire.

r_d—Total radius of single conductor wire.

Δp—Furnace pressure.

$(\rho c)_{cu}$—Sensible volumetric heat capacity of copper wire.

$(\rho c)_{\text{eff}}$—Effective sensible volumetric heat capacity of cable core.

$(\rho c)_i$—Sensible volumetric heat capacity of wire insulation.

$(\rho c)_s$—Sensible volumetric heat capacity of cable sheath.